Journal of Alloys and Compounds 502 (2010) 508–512

Contents lists available at ScienceDirect

Journal of Alloys and Compounds

journal homepage: www.elsevier.com/locate/jallcom

Synthesis of titanium diboride reinforced alumina matrix nanocomposite by mechanochemical reaction of Al–TiO_2–B_2O_3

E. Mohammad Sharifi*, F. Karimzadeh, M.H. Enayati

Department of Materials Engineering, Nanotechnology and Advanced Materials Institute, Isfahan University of Technology, Isfahan 84156-83111, Iran

ARTICLE INFO

Article history:
Received 29 November 2009
Received in revised form 26 April 2010
Accepted 28 April 2010
Available online 6 May 2010

Keywords:
Nanocomposites
Alumina
Titanium diboride
Mechanochemical processing

ABSTRACT

In order to produce alumina matrix nanocomposite reinforced by titanium diboride, a mixture of titanium oxide, boron oxide and aluminum powders was subjected to high-energy ball milling. The structural evaluation of powder particles after different milling times was studied by X-ray diffractometry, scanning electron microscopy and transmission electron microscopy. The results showed that after 60 h of milling the Al/TiO_2/B_2O_3 reacted with a self-propagating combustion mode and an alumina matrix nanocomposite containing titanium diboride particulate was formed. In final stage of milling, the crystallite size of alumina and titanium diboride were calculated to be less than 50 nm. No phase change observed after annealing treatment of the synthesized nanocomposite powders. The formation mechanism of this nanocomposite was investigated.

1. Introduction

Alumina (Al_2O_3) is a ceramic material with excellent potential properties; high melting point, high hardness, thermal stability and corrosion resistance. Such unique properties give alumina ceramics wide applications, such as wear resistant materials and cutting tools [1–5]. However, their applications as structural materials are still restricted due to their brittleness, relative low thermal shock and poor sinterability [6]. Compositing is a possible technique for decrease some of these problems [7]. Researches on the alumina-based ceramic tool materials during the past years are mainly focused on the addition of one or several of the reinforcement phases, such as TiC, TiN, TiB_2, ZrO_2, SiC, etc. into Al_2O_3 matrix [2–10]. Niihara showed that Al_2O_3-based composites reinforced with sub-micrometer or nanometer second phases have excellent mechanical properties [11].

Titanium diboride (TiB_2) is a potential choice as a second phase, because it has good structural and thermodynamic compatibility with Al_2O_3. Moreover, the TiB_2 particles exhibit very high hardness and stiffness [12]. Al_2O_3–TiB_2 composites with high wear resistance, high strength and fracture toughness, and good sinterability have drawn more attention because of their potential application in cutting tools [13].

Several techniques such as hot pressing, pressure-less sintering, self-propagating high temperature synthesis (SHS) and mechanochemical synthesis have been developed to produce a wide array of alumina matrix composites. Among these methods, mechanochemical synthesis; that is, chemical reactions induced by high-energy ball milling, is well known for fabrication of novel materials such as nanocomposites [14]. Mechanochemical processing can lead to formation of interpenetrating phase composites with nano-sized microstructures which exhibit properties and performance much improved over their conventional microcrystalline counterparts [15,16].

The reaction systems which are possible to prepare Al_2O_3–TiB_2 composites are Al–TiO_2–B, Al–B_2O_3–Ti, Al_2O_3–Ti–B and Al–TiO_2–B_2O_3. In order to decrease processing costs, Ti and B are substituted by TiO_2 and B_2O_3. The reductions of boron oxide to boron and of titanium oxide to titanium by aluminum are feasible and it can be observed from the free energy formation of TiO_2, B_2O_3 and Al_2O_3 as shown in Fig. 1 [17]. In this study, Al_2O_3–TiB_2 nanocomposite was synthesized by mechanochemical reaction between TiO_2, B_2O_3 and Al. The formation mechanism of Al_2O_3–TiB_2 nanocomposite and its thermal stability were investigated.

2. Experimental

High purity TiO_2 (rutile), B_2O_3 and Al powders were mixed according to reaction (1) to produce Al_2O_3–TiB_2 nanocomposite:

$$10Al + 3TiO_2 + 3B_2O_3 = 5Al_2O_3\,(71\ wt.\%) + 3TiB_2\,(29\ wt.\%) \quad (1)$$

$$\Delta G^{\circ}_{298} = -2633.9\ kJ/mol, \quad \Delta H^{\circ}_{298} = -2710\ kJ/mol$$

The negative value of ΔG°_{298} suggests that reaction (1) can thermodynamically takes place at room temperature. ΔH°_{298} value is also negative, indicating that this reaction is exothermic.

* Corresponding author. Tel.: +98 312 5201676; fax: +98 311 3912752.
E-mail address: e.mohamadsharifi@ma.iut.ac.ir (E. Mohammad Sharifi).

0925-8388/$ – see front matter © 2010 Elsevier B.V. All rights reserved.
doi:10.1016/j.jallcom.2010.04.207

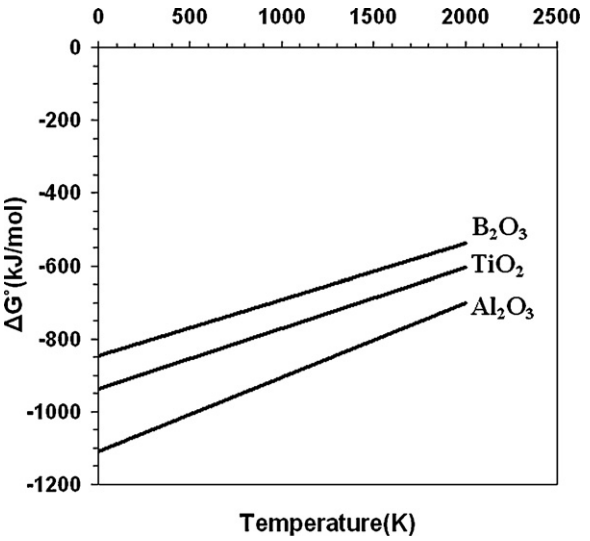

Fig. 1. Standard free energy of formation as a function of temperature for boron oxide, titanium oxide and alumina.

Ball milling of powder mixture was carried out in a planetary ball mill at room temperature and under argon atmosphere. Milling media was hardened chromium steel vial (150 ml) with five hardened carbon steel balls (20 mm). The ball-to-powder weight ratio and the rotational speed of vial were 10:1 and 500 rpm, respectively. The milling was interrupted at selected times and a small amount of powder was removed for further characterizations. Phase transformation and crystallite size evaluation during milling were determined by X-ray diffraction (XRD) in a Philips X' PERT MPD diffractometer using filtered with Cu Kα radiation (λ = 0.15406 nm). The morphology of milled powder particles was examined by scanning electron microscopy (SEM) in a Philips XL30 at an accelerating voltage of 30 kV. The sample for transmission electron microscopy (TEM) was prepared by suspending the powder sample in ethanol and subjecting it to ultrasonic vibration. A drop of the suspension was then placed on a carbon-coated copper grid and dried. The powder sample mounted on the copper grid was studied using a 120 kV Philips CM120 transmission electron microscope.

Crystallite size and internal strain of specimens were calculated from broadening of XRD peaks using the Williamson–Hall method [18].

$$\beta\cos\theta = \frac{0.9\lambda}{D} + 2\sqrt{(\varepsilon)^2}\sin\theta$$

where θ is the Bragg diffraction angle, D is the average crystallite size, ε is the average internal strain, λ is the wavelength of the radiation used and β is the diffraction peak width at half maximum intensity. The average internal strain can be estimated from the linear slope of $\beta\cos\theta$ versus $\sin\theta$, while the average crystallite size can be estimated from the intersect of this line at $\sin\theta = 0$.

Prepared Al_2O_3–TiB_2 nanocomposite powder was isothermally annealed to study the thermal behavior of as-milled powders. Powder samples were sealed and then annealed at 900 and 1200 °C for 1 h under flowing argon atmosphere in a conventional tube furnace and then cooled in air. The structural evolutions occurred during annealing were determined by XRD.

3. Results and discussion

3.1. Phase evolution and reaction mechanism

Al_2O_3–TiB_2 nanocomposite was synthesized according to reaction (1) which involves two steps. In the first step, since the Gibbs free energy of Al_2O_3 is highly lower than of both TiO_2 and B_2O_3 (Fig. 1), the aluminothermic reduction reactions take place to form Al_2O_3, elemental Ti and B as follows:

$$4Al + 3TiO_2 = 2\alpha\text{-}Al_2O_3 + 3[Ti], \quad (2)$$

$$\Delta G^\circ_{298} = -500.2\,\text{kJ/mol}, \quad \Delta H^\circ_{298} = -521.2\,\text{kJ/mol}$$

$$2Al + B_2O_3 = \alpha\text{-}Al_2O_3 + 2[B], \quad (3)$$

$$\Delta G^\circ_{298} = -416.9\,\text{kJ/mol}, \quad \Delta H^\circ_{298} = -402.7\,\text{kJ/mol}$$

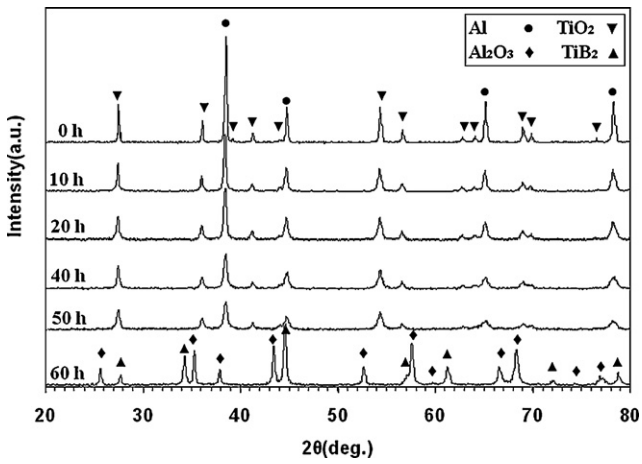

Fig. 2. XRD patterns taken from the Al/TiO_2/B_2O_3 powder mixture after different milling times.

After the first step, the released heat for exothermic reactions (2) and (3) provide the activation energy for reaction of Ti with B in the Al_2O_3 matrix as follow:

$$Ti + 2B = TiB_2, \quad (4)$$

$$\Delta G^\circ_{298} = -319.9\,\text{kJ/mol}, \quad \Delta H^\circ_{298} = -342\,\text{kJ/mol}$$

During milling in room temperature, reactions (2), (3) and (4) can thermodynamically occur due to their negative free energy change. However reactions with negative ΔG°_{298} are not necessarily occurring at room temperature because of their slow kinetic. In this regard, mechanochemical processing can enhance kinetics of reactions via (i) introducing excess energy into reactants in the form of structural defects, (ii) creating high diffusivity paths, (iii) providing extensive interface area between reactants during repeated fracturing and cold welding of powder particles and (iv) local temperature rise [15].

Fig. 2 shows the XRD patterns of powder mixture as-received and after different milling times. The diffraction pattern of initial powder mixture shows all expected peaks of Al and TiO_2. The lack of B_2O_3 peaks on XRD pattern is related to the lower intensity of B_2O_3 peaks compared to Al and TiO_2. XRD patterns of powder mixture up to 50 h of milling time were identified as a mixture of titanium oxide and aluminum. This result indicating that ball milling up to 50 h had no effect on as-received powder mixture except broadening of Bragg peaks which is caused by reduction of the crystallite size as well as microstrain induced in the powder particles. The variation of crystallite size and lattice strain of the Al and TiO_2 powders as a function of milling time, is presented in Fig. 3. Both Al and TiO_2 powders achieved a crystallite size of about 40 nm after 50 h of milling time. As expected the lattice strain of Al and TiO_2 was increased during milling time as result of increasing number of lattice defects. Reducing the crystallite size to nanometer range and increasing the defect densities can promote the reaction kinetically by providing short circuit diffusion paths [14].

XRD patterns after 60 h, showed no TiO_2 and Al peaks. Meanwhile several additional peaks corresponding to α-Al_2O_3 and TiB_2 compounds developed on XRD patterns. It is worthwhile to notice that this phase transformation was accompanied by an increase of the temperature of vial, measured by pyrometer, suggesting that a combustion reaction occurred between Al, TiO_2 and B_2O_3.

The mechanochemical reactions which can occur during milling take place in two distinct modes, i.e., either self-propagating combustion reaction or a progressive reaction. It has been demonstrated that the value of adiabatic temperature (T_{ad}) can be used as a rough

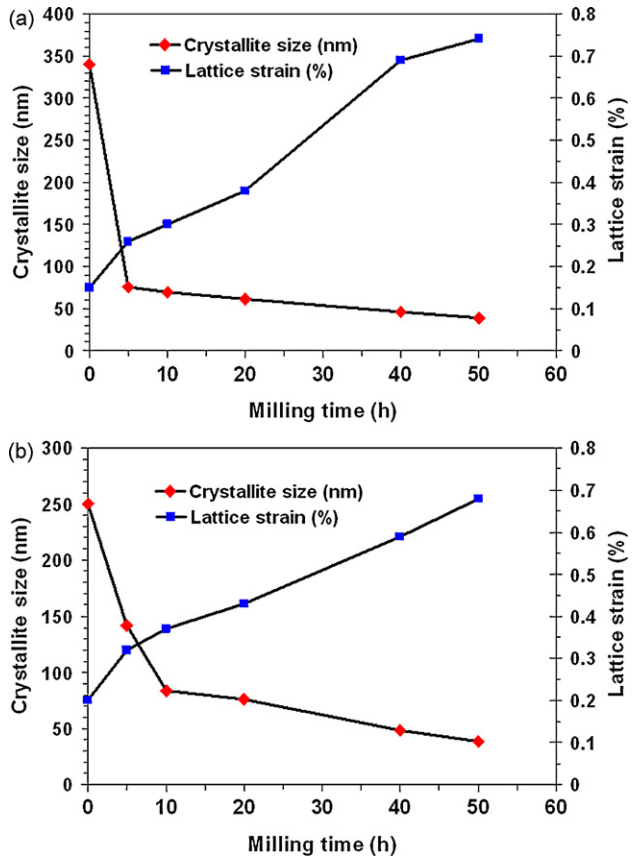

Fig. 3. Variation in crystallite size and lattice strain with milling time for: (a) Al and (b) TiO_2.

guide to the existence of combustion in milling process. T_{ad} should be above 1800 K in self-propagating combustion reaction in a thermally ignited system [19,20].

The value of T_{ad} can be calculated using following relation:

$$Q = (-\Delta H^{\circ}_{298}) = \int_{298}^{T_{ad}} \Sigma C_p(\text{Products}) dT \quad (5)$$

where Q is the heat of reaction, ΔH°_{298} is the enthalpy change at 298 K (room temperature) and C_p is the heat capacities of products.

Using relation (5) and thermodynamic data [21], the T_{ad} for reaction (1) was found to be 2812 K which is much higher than the critical value of 1800 K. Consequently, during milling of $Al/TiO_2/B_2O_3$ powder mixture, reaction (1) takes place in self-propagating combustion mode.

In combustion type reactions, there is an induction milling time after which the reaction initiates and proceeds at a high transformation rate, producing a rapid rise in temperature, which can be detected by the increased temperature at the wall of the mill vial [14,15]. As mentioned earlier as milling time was increased to about 60 h, reactions (2) and (3) occurred. The heat released from these exothermic reactions provides the activation energy for TiB_2 formation according to reaction (4).

The crystallite size and internal strain of synthesized Al_2O_3–TiB_2 nanocomposite were estimated using the Williamson–Hall method [18]. The crystallite size and mean lattice strain of Al_2O_3 and TiB_2 after 60 h of milling time were calculated to be 45 nm, 0.3% and 40 nm, 0.35%, respectively.

3.2. SEM study

Fig. 4 shows the morphology of as-received Al, TiO_2 and B_2O_3 powder particles. The aluminum powder particles were irregular in shape with a size distribution of 20–100 μm. TiO_2 powders with spherical morphology and mean particle size of 0.2 μm show a tendency to agglomeration. The B_2O_3 particles were angular in shape with a size distribution of 1–30 μm.

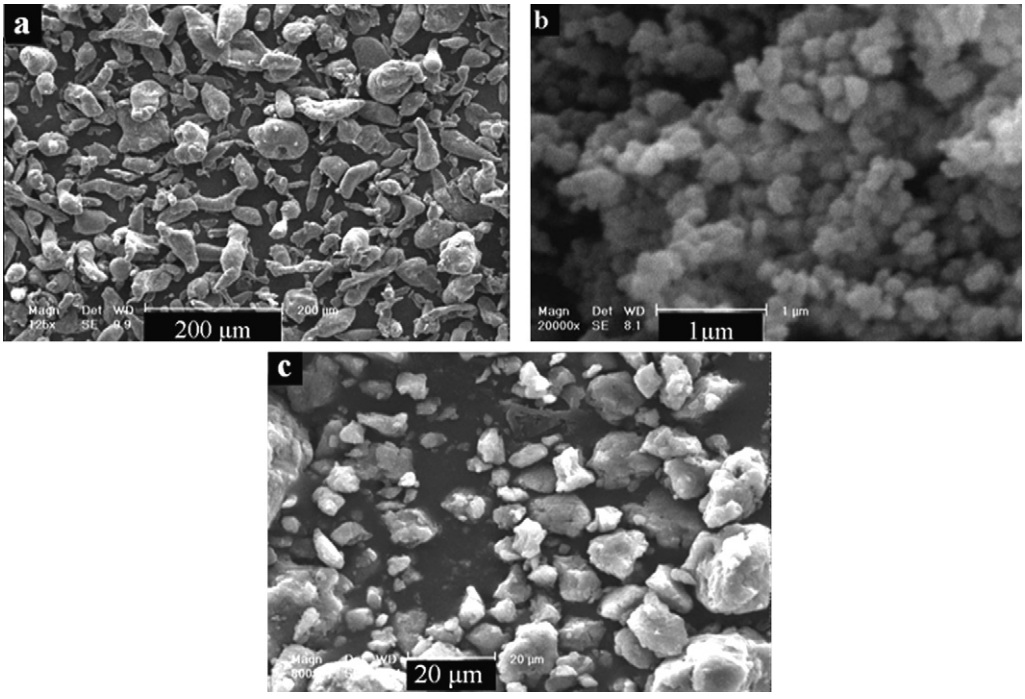

Fig. 4. SEM micrographs of as-received elemental powder particles: (a) Al, (b) TiO_2 and (c) B_2O_3.

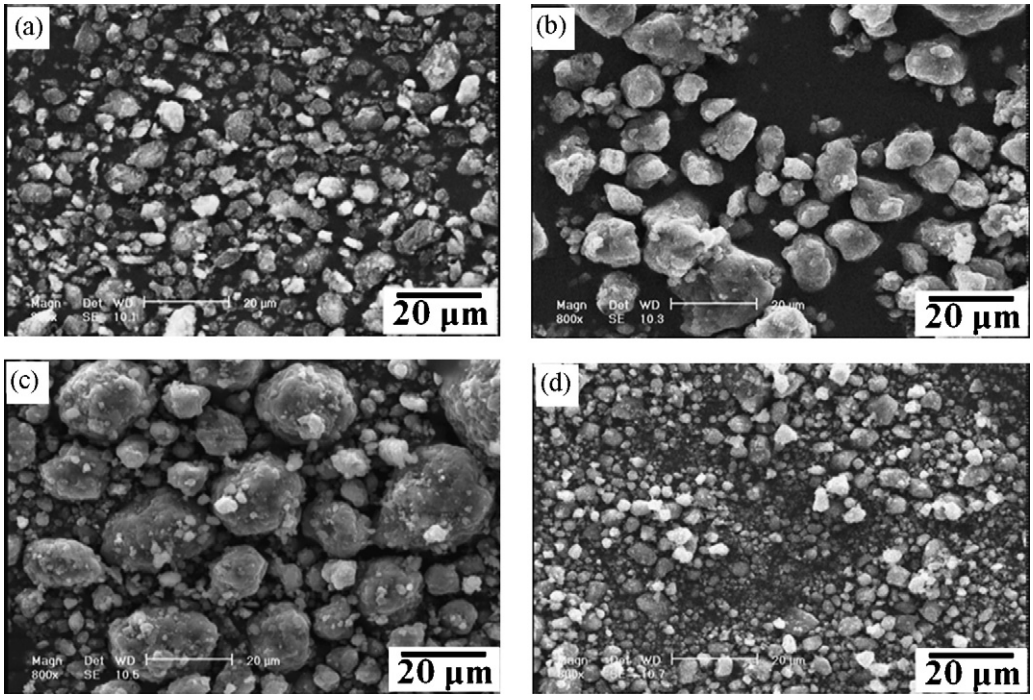

Fig. 5. SEM micrographs of Al_2O_3–TiB_2 powder particles after (a) 2 h, (b) 20 h, (c) 40 h and (d) 60 h of milling times.

The underlying mechanism of ball milling is repeated deformation, fracturing and cold welding of powder particles during collision of balls [15]. During milling of Al/TiO_2/B_2O_3 powder mixture, TiO_2 and B_2O_3 powder particles are dynamically dispersed through the ductile reductant (Al).

Fig. 5 shows morphology of powder particles after different milling times. Fig. 5a shows that after 2 h of milling the morphology of powder particles was angular with a mean particle size of about 5 μm. By increasing milling time to 20 h, the mean particle size of powders increased which was caused by cold welding phenomenon (Fig. 5b). After 40 h of milling, the morphology of powder particles was almost equiaxed with a wide size distribution of 1–30 μm (Fig. 5c). Further milling up to 60 h led to a significant decrease in powder particle size because of occurrence of combustion reaction and fragmentation of the brittle constituent phases, Al_2O_3 and TiB_2 (Fig. 5d). The powder particles after 60 h of milling are agglomerates of ultrafine particles.

3.3. TEM study

Fig. 6 shows TEM images and related selected-area diffraction pattern (SADP) of the powder milled for 60 h. Fig. 6a and b displays the bright field (BF) micrographs indicating nano-sized phases with less than 50 nm. The SADP, Fig. 6c, also indicates fine crystalline size. As can be seen, relatively good agreement exists regarding the grain size of the phases estimated from TEM observation and that from XRD analysis using Williamson–Hall method.

3.4. Thermal stability

Nanocrystalline structures are thermodynamically metastable because of the large excess free energy stored in their grain boundaries [15]. Significant grain growth was observed in several nanocrystalline materials [22,23]. Thermal stability of Al_2O_3–TiB_2 nanocomposite was investigated by annealing of ball-milled pow-

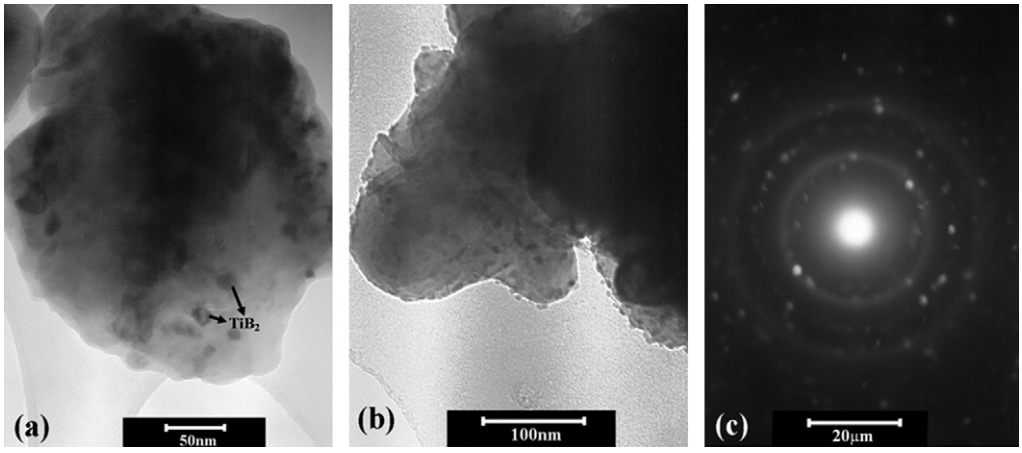

Fig. 6. TEM images ((a) and (b)) and selected-area diffraction pattern (c) of Al_2O_3–TiB_2 nanocomposite.

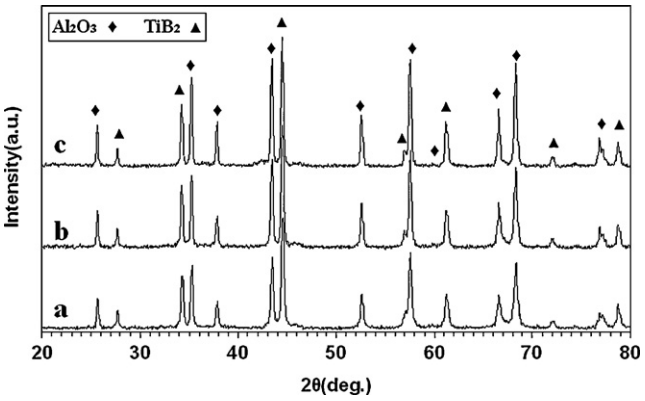

Fig. 7. The XRD patterns of Al_2O_3–TiB_2 powder (a) as-milled for 60 h; (b) and (c) after subsequent annealing at 900 and 1200 °C for 1 h.

ders at 900 °C and 1200 °C for 1 h. The XRD patterns of as-milled samples and after subsequent annealing are shown in Fig. 7.

Annealing at 900 °C caused only a slight narrowing of XRD peaks indicating that no significant crystallite growth occurred at 900 °C. In contrast, after annealing at 1200 °C the crystallite size of Al_2O_3 and TiB_2 was achieved to 80 nm and 70 nm, respectively. No additional change in phase composition occurred in powder particles after annealing.

4. Conclusions

This study investigated synthesis and characterization of Al_2O_3–TiB_2 nanocomposite by ball milling of mixture of Al, TiO_2 and B_2O_3 powders. Ball milling up to 50 h led to no phase change in as-received powder mixture except broadening of Bragg peaks which is caused by reduction of the crystallite size as well as microstrain induced in the powder particles. However, after 60 h of ball milling the reaction occurred with combustion mode and as a result Al_2O_3–TiB_2 nanocomposite formed. It was found that Al_2O_3 and TiB_2 phase had a nanocrystalline structure with a crystallite size less than 50 nm. No significant grain growth or phase change observed after annealing of 60 h milled Al_2O_3–TiB_2 powder at 900 °C and 1200 °C for 1 h.

References

[1] T. Sekine, T. Nakajima, S. Ueda, K. Nihara, J. Am. Ceram. Soc. 80 (1997) 1139–1148.
[2] C. Xua, X. Ai, C. Huang, Wear 249 (2001) 503–508.
[3] J.G. Baldoni, S.T. Buljan, Am. Ceram. Soc. Bull. 67 (1988) 381–386.
[4] X. Ai, Z.Q. Li, J.X. Deng, Key Eng. Mater. 108–110 (1995) 98–112.
[5] X.S. Li, Key Eng. Mater. 96 (1994) 1–18.
[6] J.G. Li, L. Gao, J.K. Guo, J. Eur. Ceram. Soc. 23 (2003) 69–74.
[7] W. Acchar, P. Greil, A.E. Martinelli, C.A. Cairo, A.H. Bressiani, J.C. Bressiani, J. Eur. Ceram. Soc. 20 (2000) 1765–1769.
[8] E. Mohammad Sharifi, F. Karimzadeh, M.H. Enayati, J. Alloys Compd. 482 (2009) 110–113.
[9] E. Mohammad Sharifi, F. Karimzadeh, M.H. Enayati, J. Alloys Compd. 491 (2010) 411–415.
[10] R. Tomasi, E.M.J.A. Pallone, W.J. Botta, Mater. Sci. Forum 312–314 (1999) 333–338.
[11] K. Nihara, J. Ceram. Soc. Jpn. 99 (1991) 974–982.
[12] J.F. Shackelford, W. Alexander, CRC Materials Science and Engineering Handbook, 3rd ed., CRC Press, Boca Raton, FL, 2001.
[13] M. Gu, C. Huang, S. Xiao, H. Liu, Mater. Sci. Eng. A 486 (2008) 167–170.
[14] L. Takacs, Prog. Mater. Sci. 47 (2002) 355–414.
[15] C. Suryanarayana, Prog. Mater. Sci. 46 (2001) 1–184.
[16] D.L. Zhang, Prog. Mater. Sci. 49 (2004) 537–560.
[17] E.A. Brandes, G.B. Brook, Smithells Metals Reference Book, 5th ed., Butterworth–Heinemann, 1992.
[18] K. Williamson, W.H. Hall, Acta Metall. 1 (1953) 22–31.
[19] F.W.J. Botta, R. Tomasi, E.M.J.A. Pallone, A.R. Yavari, Scr. Mater. 44 (2001) 1735–1740.
[20] B.S.B. Reddy, K. Das, S.K. Pabi, S. Das, Mater. Sci. Eng. A 445–446 (2007) 341–346.
[21] O. Kubaschewski, C.B. Alcock, Metallurgical Thermochemistry, 5th ed., Pergamon Press, 1979.
[22] R. Birringer, Mater. Sci. Eng. A 117 (1989) 33–43.
[23] T.R. Malow, C.C. Koch, Mater. Sci. Forum 225–227 (1996) 595–604.